PROCEEDINGS OF THE ROYAL SOCIETY A

Proc. R. Soc. A (2008) **464**, 1781–1800
doi:10.1098/rspa.2007.0362
Published online 25 March 2008

Deformation and rupture of lipid vesicles in the strong shear flow generated by ultrasound-driven microbubbles

By Philippe Marmottant[1,*], Thierry Biben[2,3] and Sascha Hilgenfeldt[1,†]

[1]*Faculty of Applied Physics, University of Twente, PO Box 217, 7500AE Enschede, The Netherlands*
[2]*Université de Lyon, 69000 Lyon, France*
[3]*Laboratoire PMCN, Université de Lyon 1, CNRS, UMR 5586, 69622 Villeurbanne Cedex, France*

Considering the elastic response of the membrane of a lipid vesicle (artificial cell) in an arbitrary three-dimensional shear flow, we derive analytical predictions of vesicle shape and membrane tension for vesicles close to a spherical shape. Large amplitude deviations from sphericity are described using boundary integral numerical simulations. Two possible modes of vesicle rupture are found and compared favourably with experiments: (i) for large enough shear rates the tension locally exceeds a rupture threshold and a pore opens at the waist of the vesicle and (ii) for large elongations the local tension becomes negative, leading to buckling and tip formation near a pole of the vesicle. We experimentally check these predictions in the case of strong acoustic streaming flow generated near ultrasound-driven microbubbles, such as those used in medical applications.

Keywords: lipid vesicles; shear flow; microfluidics

1. Introduction

Small gas bubbles, when placed in a sound field, are powerful actuators: their vibration, displaying a displacement amplitude much higher than that in the surrounding liquid medium, leads to strong flow fields known as acoustic streaming. Oscillating bubbles are also known for being very efficient scatterers of sound, a property used to enhance the contrast of echographic images by injecting micron-sized bubbles as contrast agents in the blood stream (see Chang *et al.* 1993; Becher & Burns 2000). In the course of such applications, mechanical effects on nearby tissues were discovered, including efficient cell membrane permeabilization in the vicinity of these bubbles (Miller & Quddus 2000; Ward *et al.* 2000), due to the opening of small pores (Taniyama *et al.* 2002). Although

* Author and address for correspondence: Laboratoire de Spectrométrie Physique, CNRS-Université Grenoble I, BP 87, 38047 Saint Martin d'Hères, France (marmotta@spectro.ujf-grenoble.fr).
† Present address: Engineering Sciences and Applied Mathematics and Department of Mechanical Engineering, Northwestern University, 2145 Sheridan Road, Evanston, IL 60208, USA.

Received 7 December 2007
Accepted 28 February 2008

This journal is © 2008 The Royal Society

the sound amplitudes in most of these experiments are very large, smaller driving pressure amplitudes below 1 bar have also proved sufficient to induce such effects (Greenleaf *et al.* 1998). This local sound-induced permeability (sonoporation) opens the perspective of *in vivo* drug delivery or gene transfer in a targeted area, where the sound is applied.

Acoustic streaming is a prime candidate for the aforementioned mechanical actuation effects. It was observed that acoustic streaming flow from gently oscillating micron-sized bubbles leads to shear forces that are sufficiently strong to rupture lipid membranes (Marmottant & Hilgenfeldt 2003). Vesicles composed of a single lipid bilayer were used as artificial cells of controlled mechanical properties in that study. The steady deformation of vesicles in simple shear flows has been well understood; it was studied numerically with boundary integral methods (Kraus *et al.* 1996) or particle dynamics methods (Noguchi & Gompper 2004), experimentally in a Couette apparatus (de Haas *et al.* 1997) or near a wall (Kantsler & Steinberg 2006; Mader *et al.* 2006), and analytically (Seifert 1999). In the present article, we will be interested in describing the vesicle membrane tension and in understanding the rupture mechanism of the membrane in *arbitrary* flow fields, including those set up in acoustic streaming.

This article is organized as follows. An analytical study of small vesicle deformation for arbitrary flow fields, focusing on the spatial dependence of membrane tension, is described in §2. The case of large deformation amplitudes is treated numerically in §3. The shear flow originating from a vibrating bubble is explained in §4. Experiments showing the elongation and rupture mechanisms of a lipid vesicle are described in §5.

2. Elongation and tension of a vesicle in a shear flow

The purpose of this section is to determine the response of the vesicle in a shear flow, in the case of arbitrary small amplitude deformations. We will focus on calculating the membrane tension and its spatial dependence along the deformed vesicle.

(*a*) *Elasticity of the membrane*

Shear stress in a liquid leads to deformation of lipid vesicle membranes, which resist the shear through membrane elasticity. The elastic properties are parametrized by an extension modulus with typical value $K_A \simeq 0.24\ \mathrm{N\,m^{-1}}$ (Boal 2002) and a bending modulus $\kappa \simeq 0.85 \times 10^{-19}$ J (Rawicz *et al.* 2000). The lipid membrane is a quasi-two-dimensional liquid; its elastic shear modulus within the membrane plane vanishes.

The total lipid area A of the vesicle can be decomposed as $A = A_\mathrm{p} + A_\mathrm{fluct}$, with A_p as the contour area of the mean shape and A_fluct as the excess area generated by thermal fluctuations. The fluctuation area at equilibrium for vanishing tensions is $A_\mathrm{fluct}/A = k_B T/8\pi\kappa \times \ln(\pi^2 R^2/6b^2) \sim 0.04$ for a vesicle of radius $R \sim 10\ \mu\mathrm{m}$, $\kappa \sim 10^{-19}$ J and $b \sim 1$ nm, a molecular scale that gives the minimum wavelength of the thermal undulations (de Haas *et al.* 1997). A_p provides a reservoir of area under shape changes.

In the shear flow, the vesicle adapts to the applied shear stress by developing a tension σ in its membrane and by deforming into an ellipsoidal shape. We define the deviation from sphericity by $\Delta A_\mathrm{p}(\sigma) = A_\mathrm{p}(\sigma) - A_\mathrm{s}$, with A_s as the area of a sphere of the same volume. At zero shear flow and near vanishing tension, the vesicle might already be deflated and have a non-vanishing ΔA_p. Under shear, this deviation will be augmented by the ironing out of fluctuations so that the global elastic response to a *homogeneous* tension σ is

$$\frac{\Delta A_\mathrm{p}(\sigma)}{A} \simeq \frac{\Delta A_0}{A} + \frac{\sigma}{K_A}. \tag{2.1}$$

The first term on the r.h.s. represents the initial area after ironing out, while the second one is due to the membrane elasticity itself.

(*b*) *Deformation and distribution of membrane tension*

(i) *Arbitrary three-dimensional linear flow*

To determine the location and triggering of membrane rupture, we now focus on the value and inhomogeneity of membrane tension, as well as the deformation. We begin with an analytical prediction at *small* deformation amplitudes, in the general case of an elongational and rotational flow. Indeed, in experiments we present, the flow is not a simple linear shear flow (where the elongation and vorticity rates are equal), but can be mainly elongational (near a stagnation point) or rotational (in a vortex centre).

We linearize an arbitrary flow field around the centre of mass location of the vesicle, i.e.

$$v_i = G_{ij} x_j + \Omega_{ij} x_j,$$

at a position x_i away from the centre, where G_{ij} is the rate of strain tensor and Ω_{ij} is the antisymmetric rotational tensor, both evaluated at the centre of the vesicle. We choose the three-dimensional vector basis ($\boldsymbol{e}_1$, $\boldsymbol{e}_2$ and $\boldsymbol{e}_3$) with coordinates (x_1, x_2 and x_3) so that G_{ij} can be written as diag(g_1, g_2 and g_3); the rotation vector associated with Ω_{ij} is $\boldsymbol{\Omega} = \Omega \boldsymbol{e}_3$ and $\boldsymbol{e}_1$ supports a larger elongational shear rate than $\boldsymbol{e}_2$, i.e. $g_1 > g_2$.

We consider the vesicles whose internal liquid has the same viscosity η as the external liquid, leading to a simple tank-treading motion of the membrane, while viscosity contrast leads to complex dynamics termed tumbling (Rioual *et al.* 2004), breathing (Misbah 2006) or trembling and swinging (Kantsler & Steinberg 2005).

The behaviour of quasi-spherical vesicles in a flow was described by Seifert (1999). He studied the coupling between the deformations of the (incompressible) membrane and the hydrodynamics of the viscous motion of the fluid inside and outside the vesicles. The inhomogeneous tension of the membrane $\sigma(\theta, \phi)$ (in spherical coordinates around the vesicle centre) and the local deviations from sphericity $r = R(1 + u(\theta, \phi))$ create forces on the fluid. Using the Stokes equation, the force equilibrium prescribes the shape deviation and interface tension. The membrane tension and shape deviations can both be expanded in spherical harmonics.

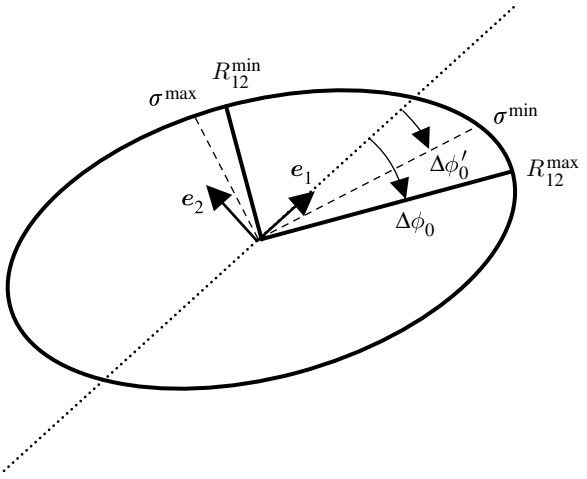

Figure 1. Schematic of the vesicle outline in the plane orthogonal to the vorticity vector $\boldsymbol{\Omega} = \Omega \boldsymbol{e}_3$. The largest elongation rate eigenvector is oriented along $\boldsymbol{e}_1$.

Here, we explicitly derive the tension distribution in addition to the shape deviation. We use the fact that, for a (three-dimensional) linear flow, the normal and divergence Lamb components defined by Seifert (1999; for the velocity field on a sphere of radius R) are equal. Such a flow gives rise to mode 2 harmonics only, and thus we can use the expressions by Seifert to obtain the resulting mode 2 harmonics for the shape and tension. The vesicle outline in the x_1x_2-plane (orthogonal to the x_3-axis of vorticity) is then an elliptic curve whose major and minor semi-axes are

$$\frac{R_{12}^{\max/\min}}{R} = 1 \pm \frac{5}{4} \frac{\eta(g_1 - g_2)R}{\sqrt{\bar{\sigma}^2 + \left(\frac{55}{12}\eta\Omega R\right)^2}} - \frac{5}{4}\frac{\eta g_3 R}{\bar{\sigma}}, \tag{2.2}$$

with $\bar{\sigma} = \sigma_{0,0} + 6\kappa/R^2$. In the following, we assume large tension compared with the curvature-induced tension ($\sigma_{0,0} \gg -6\kappa/R^2$) so that $\sigma_{0,0} \simeq \bar{\sigma}$. Given the typical values cited above, this is an excellent assumption.

The major axis is oriented under an angle $\Delta\phi_0$ with respect to the elongation x_1-axis, in the direction of the rotation $\boldsymbol{\Omega}$ (figure 1). The phase angle difference with respect to the main elongation axis is

$$\Delta\phi_0 = \frac{1}{2}\arctan\left(\frac{55}{12}\frac{\eta\Omega R}{\bar{\sigma}}\right). \tag{2.3}$$

The vesicle is extended along the rotation x_3-axis, with a semi-diameter

$$\frac{R_3}{R} = 1 + \frac{5}{2}\frac{\eta g_3 R}{\bar{\sigma}}. \tag{2.4}$$

When the rotation ratio $\eta\Omega R/\bar{\sigma}$ is very small, the directions of the vesicle extension are oriented along the elongational axis and the extensions follow the elongational rates $(R_{12}^{\max}/R) \simeq 1 + (5/2)(\eta g_1 R/\bar{\sigma})$, $(R_{12}^{\min}/R) \simeq 1 + (5/2)(\eta g_2 R/\bar{\sigma})$ and $(R_3/R) \simeq 1 + (5/2)(\eta g_3 R/\bar{\sigma})$.

The average tension $\bar{\sigma}$ is derived from the area constraint. For small deviations, the increase in the outline area is written as

$$\frac{\Delta A_{\mathrm{p}}(\bar{\sigma})}{A} = \frac{5}{6}\,\frac{(\eta(g_1-g_2)R)^2}{\bar{\sigma}^2+\left(\frac{55}{12}\eta\Omega R\right)^2} + \frac{5}{2}\,\frac{(\eta g_3 R)^2}{\bar{\sigma}^2}. \tag{2.5}$$

Equating this area increase to the elastic response (equation (2.1)) implicitly yields the average surface tension $\bar{\sigma}$ for a three-dimensional flow. Here, we assume that the average tension $\bar{\sigma}$ controls the total area extension.

Note that for vanishing rotation ratio $\eta\Omega R/\bar{\sigma}$, the area extension takes the symmetric form $\Delta A_{\mathrm{p}}/A_0 = 5/3\times\eta^2R^2(g_1^2+g_2^2+g_3^2)/\bar{\sigma}^2$, using the flow incompressibility $g_1+g_2+g_3=0$.

The liquid shear forces on the membrane are not homogeneous and promote three membrane tension harmonics, $\sigma_{2,0}$ and $\sigma_{2,\pm2}$, belonging to mode 2. In the x_1x_2-plane perpendicular to the rotation axis, the surface tension has maximum and minimum values given by

$$\frac{\sigma_{12}^{\max/\min}}{\bar{\sigma}} = 1\pm\frac{5}{4}\,\frac{\eta(g_1-g_2)R}{\bar{\sigma}}\sqrt{\frac{\bar{\sigma}^2+\left(\frac{35}{12}\eta\Omega R\right)^2}{\bar{\sigma}^2+\left(\frac{55}{12}\eta\Omega R\right)^2}} - \frac{5}{4}\,\frac{\eta g_3 R}{\bar{\sigma}}. \tag{2.6}$$

The surface tension minimum $\sigma_{12}^{\min}$ is located along an axis that makes an angle $\Delta\phi_0'$ with the x_1-axis, and which is smaller than the shape orientation angle $\Delta\phi_0$ of the largest elongation

$$\Delta\phi_0' = \frac{1}{2}\arctan\left(\frac{55}{12}\,\frac{\eta\Omega R}{\bar{\sigma}}\right) - \frac{1}{2}\arctan\left(\frac{35}{12}\,\frac{\eta\Omega R}{\bar{\sigma}}\right).$$

The surface tension maximum $\sigma_{12}^{\max}$ is located along a perpendicular axis in the same plane (figure 1). On the x_3-axis, the surface tension is locally minimal if $g_3>0$.

When rotation is small ($\eta\Omega R/\bar{\sigma}\ll1$), the relative changes in the surface tension are $(\sigma_{12}^{\min}/\bar{\sigma})\simeq-(\Delta R_{12}^{\max}/R)$, and similarly for $(\Delta\sigma_{12}^{\max}/\bar{\sigma})\simeq-(\Delta R_{12}^{\min}/R)$ and $(\Delta\sigma_3/\bar{\sigma})\simeq-(\Delta R_3/R)$. The relative changes in the surface tension are opposite to those of the extensions, while the radius maximum is located at the minimum of tension (and vice versa).

(ii) *Application to two-dimensional linear shear flow*

The small amplitude deformation of a vesicle in a shear flow was explicitly derived in the specific case of a simple plane shear $u_x=Gy$, for the case of a vesicle with thermal fluctuations but without elasticity (de Haas *et al.* 1997; Seifert 1999). Recent experiments confirmed the prediction on deformation of the shape (Kantsler & Steinberg 2005), as well as the numerical simulations (Beaucourt *et al.* 2004). Here, we derive the equations for an *extensible* elastic membrane.

In a two-dimensional linear shear flow, $u_x=Gy$, $g_1=-g_2=G/2$, $g_3=0$, $\Omega=G/2$ and the positive elongational rate eigenvector $\boldsymbol{e}_1$ makes an angle of $\pi/4$ with Ox. The deformation is described by the harmonics $u_{2,\pm2}$ only, when the spherical axis Oz is perpendicular to the flow. The contour in the xy-plane is an ellipse, whose

semi-axes are, according to equation (2.2),

$$\frac{R_{12}^{\max/\min}}{R} = 1 \pm D, \quad \text{with } D = \frac{5}{4}\frac{\eta G R}{\bar{\sigma}}, \tag{2.7}$$

while the shape is inclined by the angle $\Delta\phi_0 = (1/2)\arctan((11/6)D)$ with respect to the main elongation axis. The deformation is parametrized by only one parameter, known as the Taylor deformation parameter $D=(L-B)/(L+B)$, defined with an ellipse major axis of length L and a minor axis of length B. This equation is similar to the deformation of a liquid droplet with constant interfacial tension $\sigma_{\text{interface}}$ (Taylor 1932; see also the review article of Stone 1994 and the comparison between droplets and vesicles by Danker *et al.* in press). This extends the domain of applicability of the liquid drop model to fluctuating and extensible membranes by replacing the interfacial tension $\sigma_{\text{interface}}$ with a variable membrane tension $\bar{\sigma}$.

Rearranging the terms in equation (2.7), we note that the shear, expressed here by a shear *tension* ηGR, is counteracted by the product of the variable membrane tension $\bar{\sigma}$ and the deformation D.

The deformation implies an area increase through $D = (15/8 \times \Delta A_{\text{p}}/A)^{1/2}$. Using the elastic response of area (equation (2.1)), we obtain

$$D = \sqrt{\frac{15}{8}\left(\frac{\Delta A_0}{A} + \frac{\bar{\sigma}}{K_A}\right)}. \tag{2.8}$$

This expresses the global nonlinear 'spring-like' elastic behaviour of the vesicle, and gives the deformation D as a function of mean tension $\bar{\sigma}$.

Rewriting equation (2.7), the homogeneous variable tension as a function of shear rate is then implicitly given by

$$\frac{\bar{\sigma}}{K_A} = \frac{5}{4}\frac{Ca_K}{D(\bar{\sigma})}, \tag{2.9}$$

where we have introduced the non-dimensional quantity

$$Ca_K = \frac{\eta G R}{K_A},$$

which can be called a 'capillary number' since the extension modulus has the dimension of a capillary surface tension (Vitkova *et al.* 2004).

Thus we obtain both the tension $\bar{\sigma}$ and the deformation D as a function of Ca_K. Two regimes appear when solving equations (2.8) and (2.9): (i) a small tension regime when $\bar{\sigma}/K_A \ll \Delta A_0/A$, with the deformation being $D \simeq D_0 = (15/8 \times \Delta A_0/A)^{1/2}$ and (ii) a large tension regime when elastic increase of the lipid membrane is predominant, with the deformation tending to be $D \simeq (75/32 \times Ca_K)^{1/3}$.

The inhomogeneity of membrane tension can be given as $\sigma = \sigma_{0,0} - \Delta\sigma \sin^2\theta \cos 2(\phi - \Delta\phi_0')$, with an amplitude of variation around the average of $\Delta\sigma \simeq 5/4 \times \eta GR$ from equation (2.6), while the maximum and minimum tensions are

$$\sigma^{\max/\min} = \bar{\sigma}\left(1 \pm D\sqrt{\frac{1+(7D/6)^2}{1+(11D/6)^2}}\right). \tag{2.10}$$

The maximum occurs near the narrowest part of the vesicle (where the membrane distance to the centre is the smallest). The minimum occurs at the angle $\Delta\phi_0' = (1/2)\arctan(11/6\,D) - (1/2)\arctan(7/6\,D)$ with respect to the main elongation axis, different from the angle of the shape $\Delta\phi_0$ (figure 1). From equation (2.10), we see that $\Delta\sigma$ is proportional to D to first order.

(*c*) *Predicted modes of breakup*

We now consider the two possible scenarios for breakup, depending on the extremal values of membrane tension: either the maximum tension reaches a critical value or the minimum tension becomes negative.

(i) *Membrane rupture*

The lipid membrane cannot sustain an infinite elastic extension and above an elastic extension of approximately $\sigma_c/K_A = 3\%$, the membrane ruptures (Needham & Nunn 1990; Boal 2002). The condition for breakup ($\sigma^{\max} > \sigma_c$), which we approximate by $\bar{\sigma} > \sigma_c$ for small deformations, provides a rupture criterion based on the capillary number when using equation (2.9) and substituting $D(\bar{\sigma})$

$$Ca_K > Ca_K^c = \sqrt{\frac{6}{5}}\,\frac{\sigma_c}{K_A}\sqrt{\frac{\Delta A_0}{A} + \frac{\sigma_c}{K_A}}. \tag{2.11}$$

(ii) *Membrane buckling*

Extrapolating equation (2.10) to large amplitudes, we see that the tension might become negative near the pole, resulting in a *buckling* of the membrane. The situation $\sigma^{\min} < 0$ occurs when the deformation is larger than a critical value

$$D(\bar{\sigma}) > D^c, \tag{2.12}$$

which is approximately $D^c \simeq 1.44$ using equation (2.10). The deformation D is a growing function of Ca_K, starting from an initial value D_0, which is a function of the initial excess area. The onset of buckling is therefore expected to occur *before* rupture when the initial deformation is large enough. The purpose of §3 is to assess the validity of these predictions, which were based on small deformations (quasi-spherical shapes).

3. Deformation and distribution of tension at large amplitude: numerical calculations

(*a*) *The boundary integral method*

A convenient way to compute the dynamics of a vesicle in a Stokes flow is provided by the boundary integral method (Pozrikidis 1992). For a vesicle, the force field along the membrane and the velocity field at a point $\boldsymbol{r}$ of the membrane are related by

$$\eta \boldsymbol{v}_{\mathrm{mem}}(\boldsymbol{r}) = \int_{\mathrm{mem}} \overline{\mathsf{G}}(\boldsymbol{r} - \boldsymbol{r}')\boldsymbol{f}_{\mathrm{mem}}(\boldsymbol{r}')\,\mathrm{d}\boldsymbol{r}', \tag{3.1}$$

where $\boldsymbol{f}_{\mathrm{mem}}(\boldsymbol{r})$ is the force field applied at point $\boldsymbol{r}$ of the membrane and $\overline{\mathsf{G}}$ is the Green tensor in free space ('stokeslet'). The original three-dimensional problem can thus be reduced to a two-dimensional problem involving the membrane only.

This force field can be derived from the Helfrich curvature Hamiltonian (Helfrich & Servuss 1984),

$$H = \int_{\mathrm{mem}} \left\{ \frac{\kappa}{2}(c - c_0)^2 + \bar{\kappa} g + \sigma \right\} \mathrm{d}S, \tag{3.2}$$

where c is the local curvature of the membrane at point $\boldsymbol{r}$ ($c = c_1 + c_2$, c_1 and c_2 are the two principal curvatures at point $\boldsymbol{r}$ of the membrane); g is the Gaussian curvature ($g = c_1 c_2$) that gives rise to a constant after integration since the topology does not change and we therefore do not take into account this term; σ is the local surface tension; c_0 is an eventual spontaneous curvature that we will not consider in the following; and κ and $\bar{\kappa}$ are the curvature modulus and the Gaussian curvature modulus, respectively. The force field generated by this Hamiltonian can be calculated as

$$\boldsymbol{f}_{\mathrm{mem}} = -\kappa \left[\frac{1}{2}(c - c_0)\{c(c + c_0) - 4g\} + \Delta_{2D} c \right] \hat{\boldsymbol{n}} + \sigma c \hat{\boldsymbol{n}} + \nabla_{2D} \sigma,$$

where Δ_{2D} is the Laplace–Beltrami operator on the membrane and ∇_{2D} is the gradient operator on the membrane. The first term is the local curvature force and the second is the well-known Laplace force, while the last describes the adjustable force necessary to reduce the area towards the equilibrium. In the limit of small local area changes, the dynamics of the surface tension is given by

$$\frac{\mathrm{d}\sigma}{\mathrm{d}t} + \boldsymbol{v}_t \cdot \nabla_{2D} \sigma = \frac{K_A}{A} \frac{\mathrm{d}A}{\mathrm{d}t},$$

where $A(\boldsymbol{r})$ is the local area surrounding the point $\boldsymbol{r}$ (triangle in the computational mesh) and K_A is the area extension modulus (large so that the extension remains small).

(*b*) *Mesh advection*

We use a specific advection scheme to prevent entanglement of the mesh in the tank-treading regime due to the differential rotation between the points located in the equatorial region and the vertices located close to the rotation poles. Rather than remeshing the vesicle from time to time, which is the usual method, we prefer to modify the advection scheme so that the mesh reaches a steady state during the tank-treading motion. The mesh is advected to follow the dynamics of matter only in the normal direction, in the frame moving with the global shape of the vesicle.Where $\hat{\boldsymbol{n}}(\boldsymbol{r})$ is the outgoing normal vector at point $\boldsymbol{r}$ of the membrane, $\boldsymbol{u}_{\mathrm{rot}}$ is the solid body rotation velocity and $\boldsymbol{v}_{\mathrm{cm}}$ is the centre of mass velocity, we obtain the advection velocity in the laboratory frame as

$$\boldsymbol{v}_{\mathrm{adv}}(\boldsymbol{r}) = [\boldsymbol{v}(\boldsymbol{r}) - \boldsymbol{u}_{\mathrm{rot}}(\boldsymbol{r}) - \boldsymbol{v}_{\mathrm{cm}}] \cdot \hat{\boldsymbol{n}}(\boldsymbol{r}) \hat{\boldsymbol{n}}(\boldsymbol{r}) + \boldsymbol{u}_{\mathrm{rot}} + \boldsymbol{v}_{\mathrm{cm}}.$$

This scheme can be considered as a continuous remeshing of the vesicle.

(*c*) *Parameters*

The algorithm is implemented for a vesicle using a mesh with 642 points, obtained by refining an icosahedron and adding noise to the point positions to avoid instabilities. The vesicle is embedded in a simple two-dimensional shear flow $u_x = Gy$. The strain rate G was held constant in all computations, with a stretching 'capillary' number of $Ca_K = G/(K_A/\eta R) = 10^{-4}$ (the code was unstable for higher values), while the bending capillary number was $Ca_K = G/(\kappa/\eta R^3) = 100$, meaning that curvature effects are negligible when compared with viscous forces. The code was run with time steps of $\mathrm{d}t = 10^{-6}/(\kappa/\eta R^3)$, using a steady shear rate until a stationary shape was obtained (within 1%). The volume of the vesicle was regularly rescaled to ensure its conservation.

A given initial excess area $\Delta A_0/A$ is provided (with respect to the area, a sphere of equal volume). We prefer to express the initial excess area using $D_0 = (15/8 \times \Delta A_0/A)^{1/2}$, which directly provides the expected deformation for small strain rates in a two-dimensional flow in the small tension regime.

More commonly, the excess area is linked to the reduced volume $v_0 = V/(4\pi/3 \times (A/4\pi)^{3/2})$, comparing the actual volume V to the maximum available volume for the same area (with a sphere shape). Its expression as a function of the excess area is $v_0 = (1 + \Delta A_0/A)^{-3/2}$. We vary the initial deformation from $D_0 = 10^{-3}$ up to $D_0 = 0.95$, so that the initial reduced volumes v_0 range from 0.9999992 to 0.55.

(*d*) *Results*

Depending on the initial deflation D_0 of the vesicle, the final steady shape of the vesicle is an elongated ellipsoid (figure 2). For small deflations, the main axis of the ellipsoid is along the positive elongational axis of flow, inclined at a 45° angle with respect to the fluid velocity. This angle decreases when deflation becomes appreciable (as shown by Kraus *et al.* 1996), in accord with the deviation angle $\Delta\phi_0$ increasing with $\eta\Omega R/\bar{\sigma} \sim D$ (equation (2.3)). The longest axis of the vesicle is not an axis of symmetry; the vesicle diameter is larger in the direction orthogonal to the plane of the image, where the elongational rate from the flow is absent. At very large deformation, the shape is far from ellipsoidal, with a long central part being close to cylindrical ('cigar' shape; figure 2*d*).

The tension has minimum values near the main axis 'pole' of the vesicle and maximum values at the equator and in the plane of shear. This can be understood graphically; the shape is flattened due to the additional tension and extra area bulges out of the initial sphere due to decreased tension.

The position of the minimum tension deviates slightly from the position of the maximal values radius (figure 2*d*, the tension minimum being oriented closer to the 45° axis), a tendency predicted by the small amplitude predictions of the previous section, the deviation angle $\Delta\phi_0'$ being smaller than $\Delta\phi_0$.

The actual steady deformation was defined here using $D = (15/8 \times \Delta A/A)^{1/2}$, where the vesicle and excess areas are evaluated by fitting the vesicle mesh to an ellipsoid. We did *not* use the Taylor $D = (L-B)/(L+B)$ definition that has the inconvenience of saturating to the value 1 for large elongations. The steady deformation of vesicles in a given shear flow is found to depend strongly on initial deformation. At large $D_0 > 10^{-1}$, the steady deformation D is close to D_0, as expected. However, all initial deformations D_0, no matter how small, give rise to

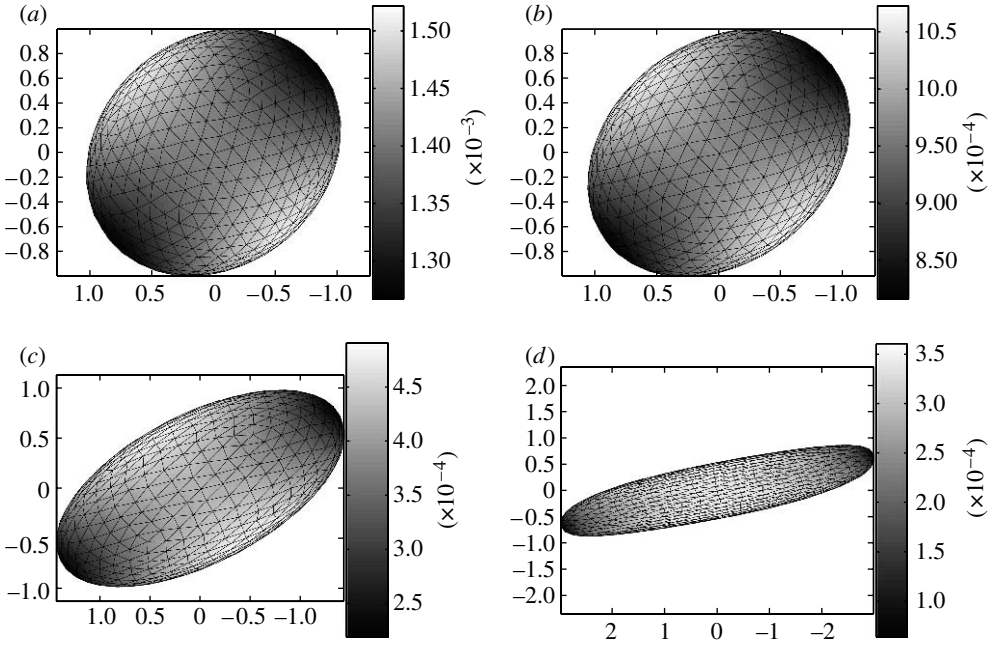

Figure 2. Numerical simulation of the steady vesicle shape and tension, in the *same* shear flow $Ca_K = 10^{-4}$, for different initial deflations (*a*) $D_0 = 10^{-2}$, (*b*) $D_0 = 0.1$, (*c*) $D_0 = 0.3694$ and (*d*) $D_0 = 0.8722$. The greyscale represents the value of σ/K_A.

a finite value for steady deformation (figure 3*a*). This effect can be understood from equation (2.9); small deformations induce strong tensions, which in-turn increase the elastic area and the actual deformation until a balance is reached, with the deformation reaching the value predicted by the large tension regime of equation (2.9). The deformation obtained from the numerical computations is slightly higher than the predicted value.

The computed average tension is inversely proportional to the actual deformation and closely follows the low-amplitude prediction (figure 3*b*), except at large deformations where the nonlinearities develop fully, resulting in a larger tension than predicted. The assumption of uniform tension, used in the liquid drop model, fails at this point.

The minimum tension tends towards the vanishing values for increasing deformation (figure 3*b*). For initial deflation parameters D_0 larger than 0.95 (v_0 smaller than 0.55), the vesicle shape becomes numerically unstable. We expect a tip-streaming-like instability to occur at this point, since the numerical shape develops a growing tip before breakdown of the calculation. Similar buckling instabilities were found on solid capsules (Lac *et al.* 2004) and on liquid droplets (Stone 1994). According to the small amplitude deformation theory, the minimum tension departs from the average with growing deformations (equation (2.10)). Extrapolating this prediction to finite values surprisingly provides a correct estimate of $\sigma^{\min}$, and predicts a vanishing tension for $D \simeq 1.44$ close to the numerical stability limit.

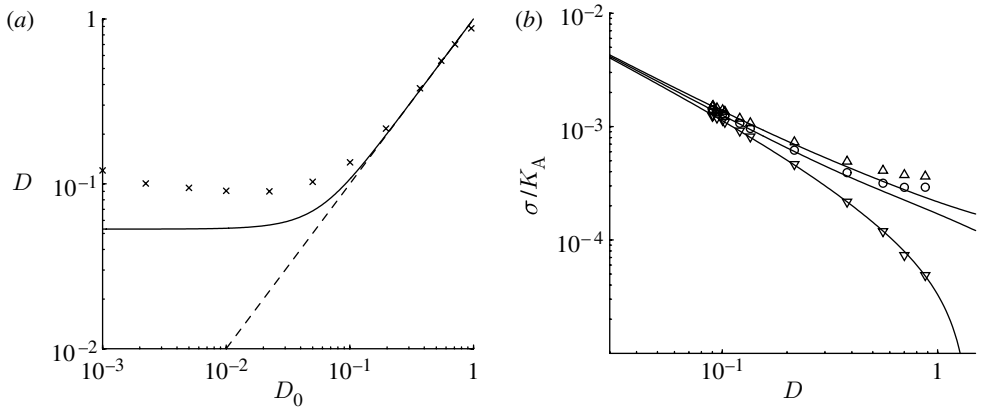

Figure 3. (*a*) Vesicle deformation, defined as $D=(15/8\times\Delta A/A_0)^{1/2}$, for different initial deformation D_0 in the same shear flow (crosses). We have plotted the predictions from the small amplitude analysis (solid line) and the prediction for inextensible membranes $D=D_0$ (dashed line). (*b*) Tension in the vesicle membrane as a function of D, indicating maximum (up triangles), mean (circles) and minimum (down triangles) values and their comparison with small amplitude deformation predictions from equations (2.9) and (2.10) (solid lines).

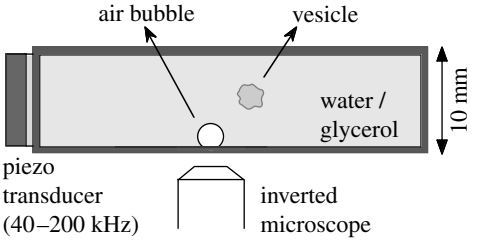

Figure 4. Experimental set-up, side view. The bubble is attached to the glass wall (dark grey line).

4. Shear flow generated near an ultrasound-driven microbubble

We now consider the description of the strong shear flow induced by the vibration of a bubble, prior to the introduction of lipid vesicles into this flow.

The set-up and the materials and methods used in the experiments are described in detail by Marmottant & Hilgenfeldt (2003, 2004). Briefly, we consider air bubbles in liquid, of radius $a=10$–100 μm, fixed by capillarity on the wall of a quartz cuvette (Hellma, Germany, $10\times10\times50$ mm). The quartz cuvette, completely filled with liquid, is excited by a piezoelectric transducer, glued to one of the cuvette walls, establishing a standing ultrasound wave field in the liquid (figure 4).

(*a*) *Recirculating acoustic streaming flow*

The fast vibration of the bubble wall, even though perfectly time-periodic, generates a steady flow; this is the acoustic streaming phenomenon. It has its origin in the inertial nonlinearity of the Navier–Stokes equations where a

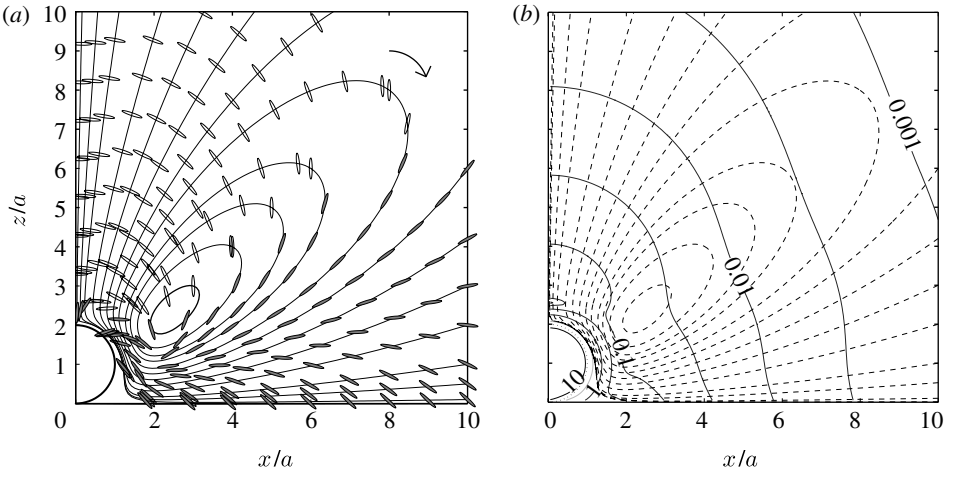

Figure 5. (*a*) Streamlines and directions of elongation due to shear strain. Filled ellipses show a transverse negative elongation, i.e. an initially spherical fluid particle is deformed into a prolate ellipsoid. Open ellipses denote positive elongation (fluid spheres are deformed into oblate ellipsoids). (*b*) Streamlines (dashed lines) and isocontours of the strain rate magnitude G in units v_0/a (solid lines). The isovalues for successive contours are, from the bubble (dots) outwards, 10, $10^{0.5}$, 1, ..., 10^{-3}.

boundary vibrating with a displacement $\epsilon \cos \omega t$ will give a velocity response whose components v_i can be expanded in ϵ as $v_i = v_{1i}\epsilon \cos \omega t + v_{2i}\epsilon^2 \cos^2 \omega t$. While the first term is time-periodic and averages out in time, the second quadratic term containing $\epsilon^2 \cos^2 \omega t = (1/2)\epsilon^2(1 + \cos 2\omega t)$ gives a steady flow, on average.

In response to sound, the bubble gently vibrates with an oscillating radius $\rho = a(1 + \epsilon' \cos(\omega t))$. Owing to the presence of the wall, the centre of mass is also translating with a position $z = \epsilon a \cos(\omega t - \Phi)$ (Marmottant *et al.* 2006*b*). The acoustic streaming flow resulting from this combination of radial and translational vibrations was described near a boundary by Marmottant & Hilgenfeldt (2003). Using this prediction, we plot streamlines near a wall in figure 5*a*.

The velocity amplitude predicted by the acoustic streaming is at most $v_0 = \epsilon\epsilon' a\omega \sin \Phi$, near the bubble wall. From the measured oscillation amplitude $\epsilon \sim \epsilon' = 0.05$ (Hansen *et al.* submitted) and the radius and frequency parameters $a = 35\ \mu\text{m}$ and $f = 67\ \text{kHz}$, we expect the maximum velocity to be of the order $6\ \text{mm s}^{-1}$ (if $\sin \Phi$ is of the order 1, in reality $\sin \Phi$ was observed to be 0.22, Marmottant *et al.* 2006*b*). The far-field dependence of the acoustic streaming velocity, decaying as r^{-3} due to the closeness of the wall, is consistent with the experimental trend. The motion is thus much localized around the bubble.

(*b*) *Strain rate generated by the flow*

The local deformation of fluid particles is characterized by the rate of strain tensor $G_{ij} = (\partial u_i/\partial x_j + \partial u_j/\partial x_i)/2$. After diagonalization, we find the elongation rate in three directions (g_1, g_2, g_3). Taking the steady streaming component of v_i as the velocity u_i, the direction of the positive elongation axis is plotted with an

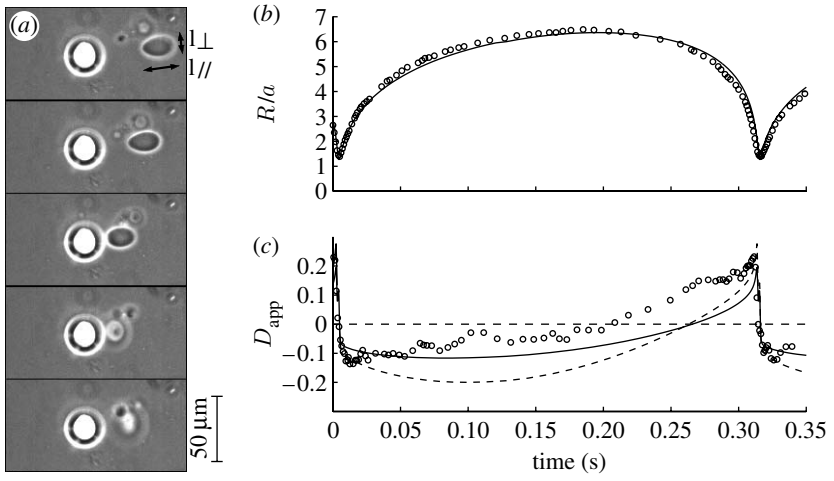

Figure 6. (*a*) Image sequence at 10 ms interframe distance (bubble is the bright object of radius $a=16$ μm, with the ultrasound frequency $f=180$ kHz); bottom view through the glass wall. (*b*) Vesicle centre to bubble centre distance during one period of the steady looping motion and (*c*) apparent deformation parameter D_{app} during the same interval. Experiments (circles) and predictions with an extensible membrane (solid line) and an inextensible membrane (dashed line).

elongated ellipse (figure 5*a*). The sign of the transverse elongation rate $g_3 = u_x/|x|$ is indicated by the filling of the ellipse. When a fluid particle is approaching the symmetry axis, the transverse elongation rate g_3 is negative. Since the other elongation axes maintain a negative and a positive elongation rate, the signs of the elongation rates are (+, − and −): an initially spherical fluid particle is deformed into a cigar-like (prolate) ellipsoid. On the other hand, when the fluid particle is going further away from the axis, the elongation rates have the signs (+, + and −): a sphere is deformed into a disc-like (oblate) ellipsoid. A fluid particle is thus found to alternately deform towards a prolate and an oblate ellipsoid during a revolution on its orbit, giving rise to the deformations observed and quantified in figure 6.

The strain rate magnitude is evaluated by the Frobenius norm of strain rate tensor, $\mathsf{G} = (g_1^2 + g_2^2 + g_3^2)^{1/2}$. The strain rate is maximal near the bubble, where it reaches a value of approximately $10v_0/a$ (figure 5*b*). The corresponding strain rate is very high, $\mathsf{G} \sim \epsilon^2\omega \sim 3\times10^3\ \mathrm{s}^{-1}$ for typical experimental values.

5. Experimental observations with vesicles

In this section, we present a variety of phenomena that are observed when the vesicles are in the vicinity of oscillating bubbles. These results qualitatively compare with and validate the predictive approach of the previous sections.

(*a*) *Materials and methods*

Lipid vesicles are injected into the liquid contained in the cuvette. We chose giant unilamellar lipid vesicles owing to their well-known mechanical properties (Rawicz *et al.* 2000; Boal 2002). Vesicles of radii 10–100 μm were grown with the

electroformation method (Dimitrov & Angelova 1987) with the lipid 1,2-dioleoyl-sn-glycero-3-phosphocoline (DOPC). We fill the vesicles with a liquid different from the outer liquid, to create an optical index contrast that results in a high contrast for phase microscopy. For this purpose, the vesicles were grown in a 0.3 M sucrose solution, plus 1 mM of the bactericide sodium azide and then transferred into an equi-osmolar glucose solution (Sandre *et al.* 1999). Their interior appears dark with phase contrast optics. Because the interior density is 4% higher, they slowly sediment and reach the bottom of the cuvette, and thus the plane of observation for an inverted microscope (Zeiss Axiovert 25CFL, Germany). For fluorescence microscopy, either the membrane or the interior liquid was marked. The membrane dye was a florescent lipid, 2-(4,4-difluoro-5,7-dimethyl-4-bora-3a, 4a-diaza-s-indacene-3-pentanoyl)-1-hexadecanoyl-sn-glycero-3-phosphocholine (β-BODIPY FL C5-HPC, Molecular Probes, The Netherlands), chosen for the similarity of its structure with DOPC. They are both glycerophospholipids, with the same phosphocholine head, and their carbon chains have comparable lengths. The liquid interior was dyed with a large weight fluorescent molecule that does not permeate through the membrane (5,6 carboxyfluorescein, Sigma Chemicals). The viscosity of the medium was adjusted by mixing the water solution with different concentrations of glycerol, providing higher viscosity solutions, up to 20 times more viscous than water.

The interaction of the bubble with vesicles was observed through the inverted microscope using phase contrast or fluorescence, and images were recorded on a digital still picture camera (Sony DSC-S75), a digital video camera (Sony DCR-PC120E) or a high-speed camera (Kodak Ektapro CR Imager, up to 2000 frames s^{-1}).

(*b*) *Vesicle deformation*

Looking perpendicularly through the glass wall on which the bubble is attached, along an axis that we call Oz, we observe an apparent periodic 'bouncing' of the vesicle on the bubble, due to the projection of the vesicle orbit. The vesicle is deformed in this process: elongated when it is approaching, compressed when it is receding (see the high-speed image sequence in figure 6 where the vesicle is out of focus in the last two images).

Seen along the axis Oz, the projected shape is roughly elliptical. This ellipse has a symmetry axis along the streamline, its extent is $l_\parallel$ along this direction and $l_\perp$ in the transverse one. The aspect ratio of the vesicle seen along Oz is estimated through the parameter $D_{\mathrm{app}} = (l_\parallel - l_\perp)/(l_\parallel + l_\perp)$ (figure 6*a*). The parameter D_{app} is positive when the vesicle looks elongated along the trajectory and negative when it looks compressed. It changes sign when the vesicle is nearest to the bubble and when the vesicle is receding from the bubble (figure 6*c*).

The shape of the vesicle evolves along its trajectory, experiencing the heterogeneous liquid strain rate distribution mapped in figure 5. We predict the vesicle shape, first by determining the streamline on which the vesicle is orbiting (solid line in figure 6*b*), then by using the theoretical principal strain rate elongations along this streamline in equation (2.5). We determine the average tension for two cases using an incompressible membrane (with an excess area of 4%) or elastic membrane with equation (2.1). From the average tension, we can determine the principal axis lengths of the ellipsoidal vesicle (R_1, R_2, R_3),

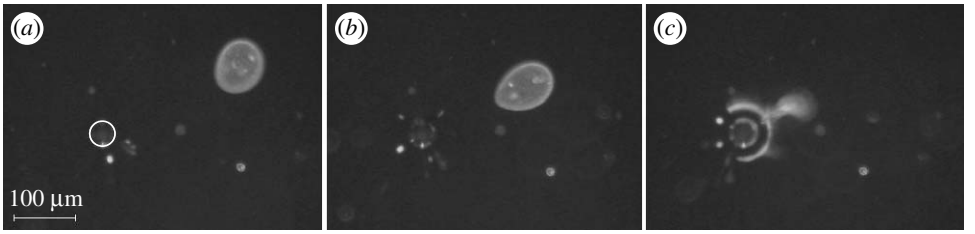

Figure 7. (*a–c*) Top view: approach of a fluorescent vesicle ($R_V \simeq 40$ µm) towards an oscillating bubble ($f = 44$ kHz), of radius $a = 20$ µm, outlined by a white circle, and its final breakup (0.25 s exposure photographs).

with R_3 the axis transverse to the trajectory plane. We project them to obtain the apparent axes $l_\perp = R_3$ and $l_\parallel = (R_1^2 \cos^2\theta + R_2^2 \sin^2\theta)^{1/2}$, with the axis tilted by θ, to obtain the apparent deformation parameter D_{app}. The predicted deformation reproduces the changes in sign and is quantitatively correct when the vesicle is close to the bubble (figure 6*c*). Using the elasticity of the membrane (solid line) instead of a fixed membrane excess (dashed line) obtains a better estimate of the vesicle shape at large distances, i.e. small strain.

(*c*) *Membrane rupture*

The deformations are enhanced in a more viscous solution and can be amplified to the point where breakup of the membrane becomes possible. In all the experiments that we present in this section, the solution is a 1 : 2 (by volume) mixture of water and glycerol, which increases the dynamic viscosity by a factor of approximately 20. Several regimes leading to membrane breakup could be observed, depending on the parameters governing the bubble oscillation dynamics.

(i) *Vesicle approaching the bubble*

A large vesicle in the viscous liquid undergoes large deformations even far away from the bubble, and its membrane eventually ruptures when the vesicle is close enough (figure 7). The shearing motion of the liquid breaks the membrane in several pieces (last image).

(ii) *Tank-treading vesicle trapped in a vortex centre*

Some vesicles can be trapped in the centre of the recirculation vortex; their position remains stationary and they only display a tank-treading motion. This attraction to the stationary line happens after a few revolutions in orbits of decreasing amplitude around the line.

The rotation frequency and deformation increase with the sound amplitude. A tip pointing towards the bubble is formed on large vesicles (figure 8), and observations with the microscope at different focusing elevations show that the tip is drawn between the bubble and the wall, as if the vesicle was aspirated there. Smaller vesicles are just elongated. Above a critical sound amplitude, the membrane cannot sustain the deformation and breaks up (not shown).

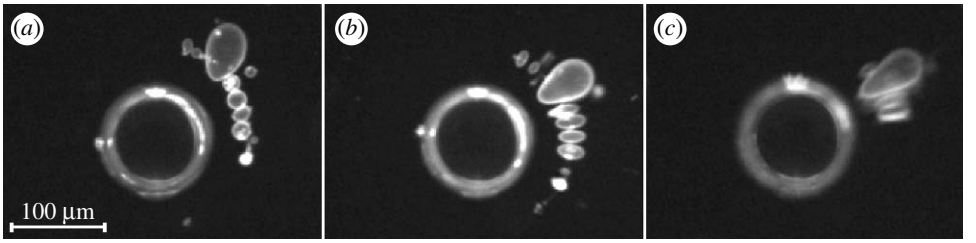

Figure 8. (*a–c*) Deformation of a *stationary* tank-treading vesicle for increasing sound amplitude ($R_V = 20$ µm) near a bubble ($a = 50$ µm, $f = 40$ kHz).

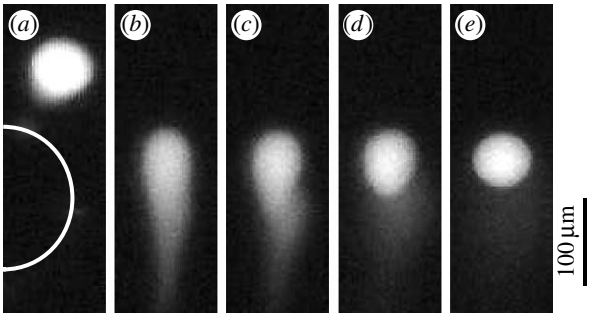

Figure 9. (*a–e*) Reversible membrane rupture when a vibrating bubble (white circle) transiently shears the vesicle ($t = 0$) and is subsequently pushed away. The internal liquid, containing a fluorescent dye, leaks out through an open pore ($t = 40$ ms to 3 s). The hole eventually closes completely ($t = 5$ s). (*a*) $t = 0$, (*b*) $t = 40$ ms, (*c*) $t = 0.5$ s, (*d*) $t = 3$ s and (*e*) $t = 5$ s.

(iii) *Reversible rupture: pore opening and closure*

The opening of a hole in a lipid membrane is not irreversible and pores can spontaneously close. As the lipid membrane is liquid in its plane, a line tension acts on the edge of a pore, effected by the exposed hydrophobic tails of the lipids. Hole opening and closure have been observed in the case of a lipid vesicle tensed by an intense illumination or adhesion to a substrate (Sandre *et al.* 1999; Brochard-Wyart *et al.* 2000). The ejection of liquid through the pore then releases the tension and the hole closes.

In our experiments, vesicles can be subject to a transient shear when an oscillating bubble, initially attached to the wall, is pushed away by acoustic pressure when the sound amplitude is suddenly increased. In this fashion, a vesicle rotating on its trajectory near a bubble experiences a strong transient shear flow that ruptures the membrane (figure 9). Some internal liquid is ejected out of this pore and dissipates quickly. The hole appears to close completely after a few seconds, as the observed leakage of dye ceases. The volume ejection can be inferred from the size reduction of the vesicle. In figure 9, we measure a volume loss of 33%.

Using equation (2.11), we estimate the capillary number for breakup to be $Ca_K^c \simeq 10^{-2}$, using $\sigma_c/K_A = 3\%$ and an initial excess area $\Delta A_0/A = 4\%$. In our experiments for small vesicles in pure water ($Ca_K \sim 10^{-4} - 10^{-3}$), the vesicle

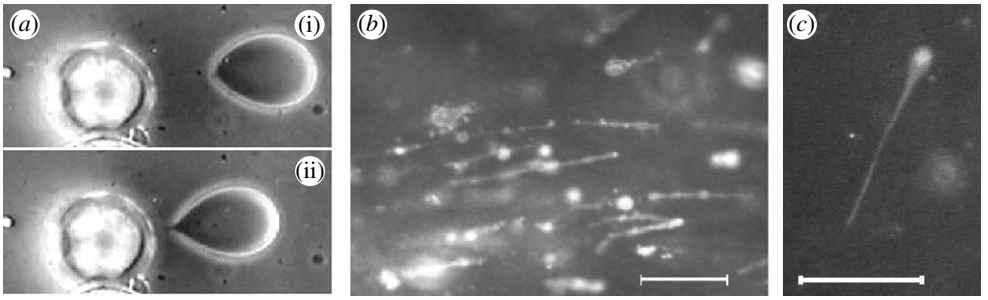

Figure 10. (*a*(i),(ii)) Cusp formation and tip streaming near a 30 μm radius bubble. (*b*) After intense cavitation at 40 kHz (the bar is 100 μm long). (*c*) Single tether pulled out of a vesicle (the bar is 100 μm long).

indeed never ruptured. In the glycerol/water mixture with $\eta = 20\eta_{\mathrm{water}}$ and large vesicles $R \sim 20$ μm, this breakup criterion is fulfilled at large sound amplitudes, where we had $G \sim 3 \times 10^3\ \mathrm{s}^{-1}$. All the observed ruptures occurred in experiments with such a large capillary number.

(*d*) *Strong localized deformation: tip and tether formation*

The membrane deformation can be localized to a small part of the vesicle. Experiments with bubbles positioned on a substrate designed with shallow holes (Marmottant *et al.* 2006*a*) showed cusp shapes and tip streaming of the vesicles (figure 10*a*). This appears to be a case where breakup is preferred through negative tension and buckling localized at the tip of the vesicle.

At high acoustic pressures, negative pressure (tension) in the liquid results in spontaneous formation of small bubbles (cavitation). These bubbles travel fast in the bulk and abruptly change directions. Exposing a solution of lipid vesicles to cavitation produces a different kind of vesicle deformation and their shape is turned into long tubes (figure 10*b*). The remaining initial vesicle can be seen on one end of these tubes (figure 10*c*), where the tube is a tether pulled out of the vesicle by the large hydrodynamic shear stresses around the moving bubbles.

The extension of a vesicle into a tube was observed by Shahidzadeh *et al.* (1998), but for low ($0.5\ \mathrm{s}^{-1}$) constant shear rates. The tube can be a stable shape for the membrane if it is tensionless, especially if its radius is close to the spontaneous curvature radius of the membrane (Rossier *et al.* 2003). Here, a tension is still present in the membrane and results in a pearling instability (Bar-Ziv & Moses 1994) that is visible in figure 10*b*.

Compared with the previous experimental situation that never resulted in such a tether formation, the difference is the size of the cavitation bubbles, which are much smaller than the vesicle (their apparent diameter when they travel fast in front of the objective is less than 10 μm), the high intensity of their oscillation and the speed of their translation. This tether formation process is similar to the local application of a point force with optical tweezers that is used to pull out the membrane out of an initially spherical vesicle (Fygenson *et al.* 1997; Powers *et al.* 2002).

From theory, the tension is expected to vanish at a specific location of the membrane when the deformation is large enough (see §2). In practice, vesicles are not sufficiently deflated initially to reach the large critical deformations

determined by the numerical calculation. Tip formation is, however, expected to occur more easily when the shear flow is not homogeneous but is stronger near one end of the vesicle. In this case, the flow cannot be linearized and the previous analysis does not hold any more. This occurs when the vesicle is very close to a bubble where the flow field is inhomogeneous on scales smaller than the vesicle size (figure 10*a*). The same small-scale argument applies to the more extreme case of tether-pulling.

6. Conclusions and perspectives

Gentle oscillations of microbubbles attached to a wall generate intense acoustic streaming flows. Soft objects, such as lipid vesicles, experience a high shear stress in the streaming, which deforms their outline and generates membrane tension that varies in time and space. The theoretical analysis in a linearized shear flow shows that the membrane tension has a maximum near the minor axis (the 'waist' of the vesicle) and a minimum near the major axis. The average tension determines the overall shape. The membrane is expected to rupture at the waist when the maximum tension reaches a critical value (controlled by the capillary number Ca_K). On the other hand, the minimum tension can become so small that it nearly vanishes (which occurs for large enough deformation D), leading to buckling and a tip-streaming-like process of local membrane extension. Tip streaming is expected to occur before breakup for deflated vesicles, i.e. those with sufficient initial excess surface area or in sufficiently inhomogeneous shear flows.

Upon breakup of vesicles, pores are nucleated and interior and exterior fluids are exchanged. In the case of living cells, these pores are believed to be at the origin of enhanced drug delivery or gene transfer when diagnostic ultrasound is applied (sonoporation). However, the acoustic streaming flows are much more controlled and have much smaller peak stresses than cavitating bubbles in ultrasound diagnostics, which often undergo violent collapses and damage cells indiscriminately. Note that the ultrasound amplitudes used in medical ultrasound are typically in the MPa range, while the typical amplitudes in our streaming experiments are below 10 kPa. Nevertheless, we demonstrated pore opening in lipid membranes, and preliminary experiments have shown that the membrane of HeLa cancer cells can also be lysed in the streaming flow near microbubbles. Further tests will determine whether the pore opening can be gentle enough to allow cell repair and survival. The effect of low-intensity ultrasound on vesicles and cell rupture indicates that more controlled experiments are possible *in vitro* and *in vivo*. We have shown that violent bubble collapses are not necessary for the rupture of membranes, and thus for transfection.

The shear flow is focused on very small volumes because the acoustic streaming velocity of the bubble decays rapidly as r^{-3}. Consequently, the shear stresses decay even faster. The focusing turns the energy in a mm-wavelength ultrasound driving into an incisive tool on the micron scale, effectively establishing microacoustic effects with low-frequency ultrasound. Micrometre-scale forces can thus be exerted on small objects such as cells, to push, deform or break them. With microacoustic tools, new potential applications in microfluidic devices arise, such as a single-cell manipulation, acoustic probing and permeabilization.

We would like to thank Detlef Lohse for his support, and Claus-Dieter Ohl and Rudiger Toegel for their help while the experimental work was performed at the University of Twente. We enjoyed fruitful discussions with Gerrit Danker, David Hansen and Manouk Abkarian.

References

Bar-Ziv, R. & Moses, E. 1994 Instability and "pearling" states produced in tubular membranes by competition of curvature and tension. *Phys. Rev. Lett.* **73**, 1392–1395. (doi:10.1103/PhysRevLett.73.1392)

Beaucourt, J., Rioual, F., Seon, T., Biben, T. & Misbah, C. 2004 Steady to unsteady dynamics of a vesicle in a flow. *Phys. Rev. E* **69**, 011 906–011 917. (doi:10.1103/PhysRevE.69.011906)

Becher, H. & Burns, P. 2000 *Handbook of contrast echocardiography*. Berlin, Germany: Springer.

Boal, D. 2002 *Mechanics of the cell*. Cambridge, UK: Cambridge University Press.

Brochard-Wyart, F., de Gennes, P. & Sandre, O. 2000 Transient pores in stretched vesicles: role of leak-out. *Physica A* **278**, 32–51. (doi:10.1016/S0378-4371(99)00559-2)

Chang, D. C., Chassey, B. M., Saunders, J. A. & Sowers, A. E. 1993 *Advances in echo imaging using contrast enhancement*. Dordrecht, The Netherlands: Kluwer Academic.

Danker, G., Verdier, C. & Misbah, C. In press. Rheology and dynamics of vesicle suspension in comparison with droplet emulsion. *J. Non-Newtonian Fluid Mech.* (doi:10.1016/j.jnnfm.2007.07.005)

de Haas, K. H., Blom, C., van de Ende, D., Duits, M. H. G. & Mellema, J. 1997 Deformation of giant lipid vesicles in shear flow. *Phys. Rev. E* **56**, 7132–7137. (doi:10.1103/PhysRevE.56.7132)

Dimitrov, D. S. & Angelova, M. I. 1987 Lipid swelling and liposome formation on solid surfaces in external electric fields. *Prog. Colloid Polym. Sci.* **73**, 48–56. (doi:10.1007/3-798-50724-4_62)

Fygenson, D. K., Marko, J. F. & Libchaber, A. 1997 Mechanics of microtubule-based membrane extension. *Phys. Rev. Lett.* **79**, 4497–4500. (doi:10.1103/PhysRevLett.79.4497)

Greenleaf, W. J., Bolander, M. E., Sarkar, G., Goldring, M. B. & Greenleaf, J. F. 1998 Artificial cavitation nucleai significantly enhance acoustically induced cell transfection. *Ultrasound Med. Biol.* **24**, 587–595. (doi:10.1016/S0301-5629(98)00003-9)

Hansen, D., Marmottant, P., Tsai, J.-C. & Hilgenfeldt, S. Submitted. Steady streaming from surface-adsorbed microbubbles.

Helfrich, W. & Servuss, R.-M. 1984 Undulations steric interaction and cohesion of fluid membranes. *Nuevo Cimento D* **3**, 137–151. (doi:10.1007/BF02452208)

Kantsler, V. & Steinberg, V. 2005 Orientation and dynamics of a vesicle in tank-treading motion in shear flow. *Phys. Rev. Lett.* **95**, 258 101–258 104. (doi:10.1103/PhysRevLett.95.258101)

Kantsler, V. & Steinberg, V. 2006 Transition to tumbling and two regimes of tumbling motion of a vesicle in shear flow. *Phys. Rev. Lett.* **96**, 036 001–036 004. (doi:10.1103/PhysRevLett.96.036001)

Kraus, M., Wintz, W., Seifert, U. & Lipowsky, R. 1996 Fluid vesicles in shear flow. *Phys. Rev. Lett.* **77**, 3685–3688. (doi:10.1103/PhysRevLett.77.3685)

Lac, E., Barthès-Biesel, D., Pelekasis, N. A. & Tsamopoulos, J. 2004 Spherical capsules in three-dimensional unbounded stokes flows: effect of the membrane constitutive law and onset of buckling. *J. Fluid Mech.* **516**, 303–334. (doi:10.1017/S002211200400062X)

Mader, M., Vitkova, V., Abkarian, M., Viallat, A. & Podgorski, T. 2006 Dynamics of viscous vesicles in shear flow. *Eur. Phys. J. E-Soft Matter* **19**, 389–397. (doi:10.1140/epje/i2005-10058-x)

Marmottant, P. & Hilgenfeldt, S. 2003 Controlled vesicle deformation and lysis by single oscillating bubbles. *Nature* **423**, 153–156. (doi:10.1038/nature01613)

Marmottant, P. & Hilgenfeldt, S. 2004 A bubble-driven microfluidic transport element for bioengineering. *Proc. Natl Acad. Sci. USA* **101**, 9523–9527. (doi:10.1073/pnas.0307007101)

Marmottant, P., Raven, J. P., Gardeniers, H., Bomer, J. G. & Hilgenfeldt, S. 2006*a* Microfluidics with ultrasound-driven bubbles. *J. Fluid Mech.* **568**, 109–118. (doi:10.1017/S0022112006002746)

Marmottant, P., Versluis, M., de Jong, N., Hilgenfeldt, S. & Lohse, D. 2006*b* High-speed imaging of an ultrasound-driven bubble in contact with a wall: "narcissus" effect and resolved acoustic streaming. *Exp. Fluids* **41**, 147–153. (doi:10.1007/s00348-005-0080-y)

Miller, D. L. & Quddus, J. 2000 Sonoporation of monolayer cells by diagnostic ultrasound activation of contrast-agent gas bodies. *Ultrasound Med. Biol.* **26**, 661–667. (doi:10.1016/S0301-5629(99)00170-2)

Misbah, C. 2006 Vacillating breathing and tumbling of vesicles under shear flow. *Phys. Rev. Lett.* **96**, 028 104. (doi:10.1103/PhysRevLett.96.028104)

Needham, D. & Nunn, R. S. 1990 Elastic deformation and failure of lipid bilayer membranes containing cholesterol. *Biophys. J.* **58**, 997–1009.

Noguchi, H. & Gompper, G. 2004 Fluid vesicles with viscous membranes in shear flow. *Phys. Rev. Lett.* **93**, 258 102–258 104. (doi:10.1103/PhysRevLett.93.258102)

Powers, T. R., Huber, G. & Goldstein, R. E. 2002 Fluid-membrane tethers: minimal surfaces and elastic boundary layers. *Phys. Rev. E* **65**, 041 901. (doi:10.1103/PhysRevE.65.041901)

Pozrikidis, C. 1992 *Boundary integral and singularity methods for linearized viscous flow*. Cambridge, UK: Cambridge University Press.

Rawicz, W., Olbrich, K., McIntosh, T., Needham, D. & Evans, E. 2000 Effect of chain length and unsaturation on elasticity of lipid bilayers. *Biophys. J.* **79**, 328–339.

Rioual, F., Biben, T. & Misbah, C. 2004 Analytical analysis of a vesicle tumbling under a shear flow. *Phys. Rev. E* **69**, 061 914. (doi:10.1103/PhysRevE.69.061914)

Rossier, O., Cuvelier, D., Borghi, N., Puech, P., Derenyi, I., Buguin, A., Nassoy, P. & Brochard-Wyart, F. 2003 Giant vesicles under flows: extrusion and retraction of tubes. *Langmuir* **19**, 575–584. (doi:10.1021/la026236t)

Sandre, O., Moreaux, L. & Brochard-Wyart, F. 1999 Dynamics of transient pores in stretched vesicles. *Proc. Natl Acad. Sci. USA* **96**, 10 591–10 596. (doi:10.1073/pnas.96.19.10591)

Seifert, U. 1999 Fluid membranes in hydrodynamic flow fields: formalism and an application to fluctuating quasispherical vesicles in shear flow. *Eur. Phys. J. B* **8**, 405–415. (doi:10.1007/s100510050706)

Shahidzadeh, N., Bonn, D., Aguerre-Chariol, O. & Meunier, J. 1998 Large deformations of giant floppy vesicles in shear flow. *Phys. Rev. Lett.* **81**, 4268–4271. (doi:10.1103/PhysRevLett.81.4268)

Stone, H. A. 1994 Dynamics of drop deformation and breakup in viscous fluids. *Annu. Rev. Fluid Mech.* **26**, 65–102. (doi:10.1146/annurev.fl.26.010194.000433)

Taniyama, Y. *et al.* 2002 Local delivery of plasmid DNA into rat carotid artery using ultrasound. *Circulation* **105**, 1233–1239. (doi:10.1161/hc1002.105228)

Taylor, G. I. 1932 The viscosity of fluid containing small drops of another fluid. *Proc. R. Soc. A* **138**, 41–48. (doi:10.1098/rspa.1932.0169)

Vitkova, V., Mader, M. & Podgorski, T. 2004 Deformation of vesicles flowing through capillaries. *Europhys. Lett.* **68**, 398–404. (doi:10.1209/epl/i2004-10211-9)

Ward, M., Wu, J. & Chiu, J.-F. 2000 Experimental study of the effects of optison® concentration on sonoporation *in vitro*. *Ultrasound Med. Biol.* **26**, 1169–1175. (doi:10.1016/S0301-5629(00)00260-X)